This article was downloaded by: [Koninklijk Meteorological Institute van]
On: 09 October 2013, At: 02:29
Publisher: Taylor & Francis
Informa Ltd Registered in England and Wales Registered Number: 1072954 Registered office: Mortimer House, 37-41 Mortimer Street, London W1T 3JH, UK

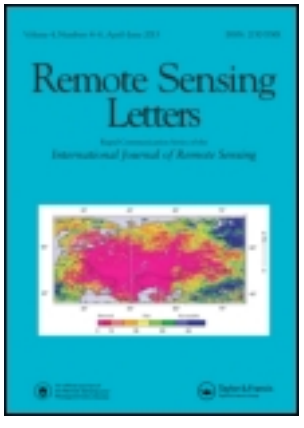

Remote Sensing Letters
Publication details, including instructions for authors and subscription information:
http://www.tandfonline.com/loi/trsl20

Evidence of pre-launch characterization problem of Meteosat-7 visible spectral response

I. Decoster[ab], N. Clerbaux[a], Y. M. Govaerts[c], E. Baudrez[a], A. Ipe[a], S. Dewitte[a], S. Nevens[a], A. Velazquez Blazquez[a] & J. Cornelis[b]

[a] Department of Observations, Royal Meteorological Institute of Belgium, Brussels, Belgium

[b] Department of Electronics and Informatics (ETRO), Vrije Universiteit Brussel, Brussels, Belgium

[c] Govaerts Consulting, Brussels, Belgium

Published online: 20 Aug 2013.

To cite this article: I. Decoster, N. Clerbaux, Y. M. Govaerts, E. Baudrez, A. Ipe, S. Dewitte, S. Nevens, A. Velazquez Blazquez & J. Cornelis (2013) Evidence of pre-launch characterization problem of Meteosat-7 visible spectral response, Remote Sensing Letters, 4:10, 1008-1017, DOI: 10.1080/2150704X.2013.828181

To link to this article: http://dx.doi.org/10.1080/2150704X.2013.828181

PLEASE SCROLL DOWN FOR ARTICLE

Taylor & Francis makes every effort to ensure the accuracy of all the information (the "Content") contained in the publications on our platform. However, Taylor & Francis, our agents, and our licensors make no representations or warranties whatsoever as to the accuracy, completeness, or suitability for any purpose of the Content. Any opinions and views expressed in this publication are the opinions and views of the authors, and are not the views of or endorsed by Taylor & Francis. The accuracy of the Content should not be relied upon and should be independently verified with primary sources of information. Taylor and Francis shall not be liable for any losses, actions, claims, proceedings, demands, costs, expenses, damages, and other liabilities whatsoever or howsoever caused arising directly or indirectly in connection with, in relation to or arising out of the use of the Content.

This article may be used for research, teaching, and private study purposes. Any substantial or systematic reproduction, redistribution, reselling, loan, sub-licensing, systematic supply, or distribution in any form to anyone is expressly forbidden. Terms &

Conditions of access and use can be found at http://www.tandfonline.com/page/terms-and-conditions

Downloaded by [Koninklijk Meteorlogical Institute van] at 02:29 09 October 2013

Remote Sensing Letters, 2013
Vol. 4, No. 10, 1008–1017, http://dx.doi.org/10.1080/2150704X.2013.828181

Taylor & Francis
Taylor & Francis Group

Evidence of pre-launch characterization problem of Meteosat-7 visible spectral response

I. DECOSTER*†‡, N. CLERBAUX†, Y. M. GOVAERTS§, E. BAUDREZ†, A. IPE†, S. DEWITTE†, S. NEVENS†, A. VELAZQUEZ BLAZQUEZ† and J. CORNELIS‡

†Department of Observations, Royal Meteorological Institute of Belgium, Brussels, Belgium

‡Department of Electronics and Informatics (ETRO), Vrije Universiteit Brussel, Brussels, Belgium

§Govaerts Consulting, Brussels, Belgium

(*Received 30 May 2013; accepted 19 July 2013*)

Since the early 1980s, the geostationary Meteosat instruments have been observing the earth at a high temporal and spatial resolution. The data record contains more than 30 years of observations and has become very useful for climate monitoring. With a compilation of 10 satellites, it is crucial to reach the highest possible consistency between the instruments. However, the quality of the level 1 data records is still far from what is needed to generate homogeneous climate data records, due to both temporal ageing as well as discontinuities between successive instruments. In this letter, a method is proposed to assess the pre-launch Meteosat-7 visible spectral response curve and a model of its ageing. The results not only validate the ageing model, but also provide evidence that the official pre-launch spectral response curve of Meteosat-7 poorly represents the sensitivity of the instrument in the blue part of the visible spectrum. Until the Meteosat-7 visible spectral response curve has been reassessed, it is suggested to replace the Meteosat-7 curve with the curve of the high resolution visible channel of Meteosat-8. Quantitatively, the error introduced when unfiltering the data (i.e. conversion from filtered to unfiltered radiance), due to the uncertainty on the Meteosat-7 spectral response, is estimated at 4.5% using the Meteosat-7 spectral response curve, but could be reduced to 2.1% by following the recommendations in this letter.

Downloaded by [Koninklijk Meteorlogical Institute van] at 02:29 09 October 2013

1. Introduction

The past decades have witnessed an increasing interest in long and consistent data records of different kinds of variables in support of climatological studies. Observations from space instruments are playing an important role in this field. The Meteosat satellites are a series of geostationary weather satellites, currently operated by the European Organisation of Meteorological Satellites (EUMETSAT), providing observations in the visible, water vapour, and infrared bands. The time length of observations exceeds the typical duration of 30 years needed to investigate climatological trends and variabilities (Duvel and Kandel 1985, Desbois *et al.* 1988, Ba and

*Corresponding author. Email: ilse.decoster@meteo.be

© 2013 Taylor & Francis

Downloaded by [Koninklijk Meteorlogical Institute van] at 02:29 09 October 2013

Nicholson 1998, Govaerts and Lattanzio 2008). Therefore, the Meteosat data also play an important role within the EUMETSAT Climate Monitoring Satellite Application Facility (CM SAF, Schulz *et al.* (2009)), as demonstrated in Roebeling *et al.* (2006), Müller *et al.* (2006), Dürr *et al.* (2010), Posselt *et al.* (2012).

In addition to a sufficiently long data record, consistency over the full time period is mandatory. However, several problems (e.g. ageing effects, lack of pre-launch characterization, . . .) prevent the use of the Meteosat first generation time series, starting in 1981 with Meteosat-2, for climate monitoring purposes. The visible channel, one of the three channels of the Meteosat Visible and Infrared Imager (MVIRI) on board of these satellites, for example, has proven to be sensitive to ageing, resulting in a decrease of signal in time. In view of its use for climate studies and as input for reanalysis, EUMETSAT recalibrated the full data set (Govaerts *et al.* 2001, 2004), assuming the decrease in signal to be grey (i.e. uniform over the full wavelength spectrum). However, the ageing appears to be scene-type-dependent, indicating that it is strongest in the blue part of the visible spectrum (Govaerts *et al.* 2004). Recently, Decoster *et al.* (2013) proposed a mathematical model describing how the spectral response curve $\phi(\lambda, t)$ looks like at a certain time t and wavelength λ compared to its pre-launch counterpart $\phi(\lambda, 0)$

$$\phi(\lambda, t) = \phi(\lambda, 0)\left(e^{-\alpha t} + \beta\left(1 - e^{-\alpha t}\right)\right)(1 + \gamma t\,(\lambda - \lambda_0)) \tag{1}$$

where λ_0 is the central wavelength of $\phi(\lambda, 0)$. The model parameter α represents the grey ageing, β represents the asymptotic sensitivity, and γ represents the spectral ageing. For Meteosat-7, it was possible to model the spectral decrease in signal using the values $\alpha = 33.2 \times 10^{-5}\text{day}^{-1}$, $\beta = 0.752$, and $\gamma = 11.8 \times 10^{-5}\mu\text{m}^{-1}\text{day}^{-1}$. Figure 1(a) shows both the pre-launch spectral response curve of the Meteosat-7 visible channel and how the curve is modelled after 8 years according to Equation (1).

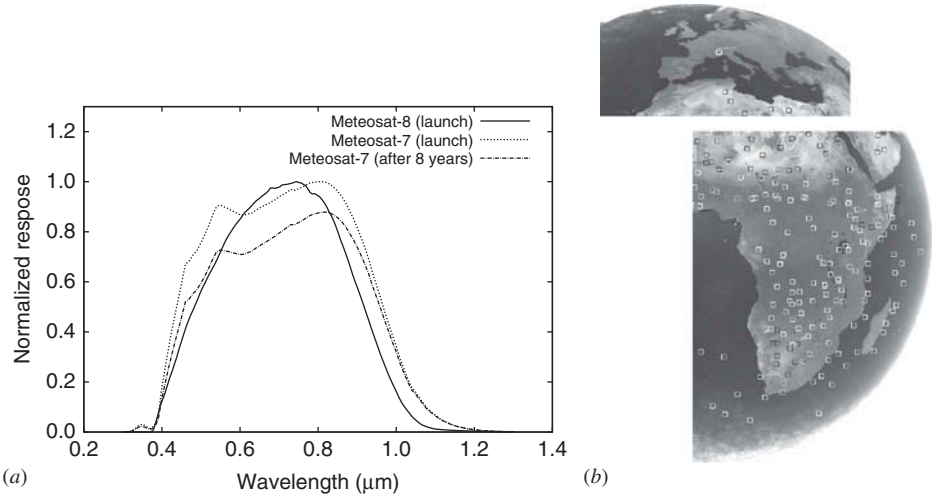

Figure 1. (*a*) Spectral response curves of the visible channel of: Meteosat-8 HRV, Meteosat-7 at launch and Meteosat-7 after 8 years in orbit according to the spectral ageing model of equation (1). (*b*) The position of the 219 clear-sky targets in the 1200 UTC HRV field of view.

Govaerts (1999) already pointed out that the original pre-launch characterization of the Meteosat-5 and -6 visible bands provides inconsistent calibration results according to the spectral behaviour of the observed targets. Since the Meteosat-5 to -7 radiometers were produced in the same batch, he suggested to use the Meteosat-7 spectral response curve for the characterization of the visible band of any radiometers of this batch.

From 2004 onwards, with the launch of Meteosat-8, a new design has been used for the Meteosat second generation satellites (Schmetz *et al.* 2002), with the 12 channel Spinning Enhanced Visible and Infrared Imager (SEVIRI) as the follow-up of MVIRI. Requirements were put on the instrument stability, where the long-term drift of the visible channels should not exceed 2% of the maximum dynamic range (Govaerts and Clerici 2003). The successor of the visible channel of Meteosat-7 is called the high resolution visible (HRV) channel, which also makes use of silicon detectors and has a similar bandpass filter as the Meteosat-7 visible channel (see the spectral response curve in figure 1(*a*)). In this letter, simultaneous Meteosat-7 visible and Meteosat-8 HRV observations are used for a post-launch assessment of the Meteosat-7 spectral response $\phi(\lambda, 0)$. It is based on the analysis of time series acquired over spectrally different earth targets, and reveals clear pre-launch characterization problems.

2. Data and methodology

In this work, 1200 UTC observations from Meteosat-7 and Meteosat-8 are compared during the period from February 2004 to July 2006 when both instruments were operational: Meteosat-7 was positioned at 0° longitude whereas Meteosat-8 was positioned at –3.4° longitude. The Meteosat-8 HRV observations are used as a reference to validate the Meteosat-7 visible spectral response curve, since the Meteosat-8 HRV curve is the follow-up of the Meteosat-7 visible one and Meteosat-8 has been better characterized. The limited ageing of Meteosat-8 is expected to still be linear as the overlap period is close to its launch date, and is accounted for as explained hereafter.

Similarly to Decoster *et al.* (2013), six time series are created for scene types with different spectral characteristics. The first one corresponds to deep convective clouds (DCC), selected from the inter-tropical convergence zone. Their nearly Lambertian reflectances and predictable albedos (Vermote and Kaufman 1995, Doelling *et al.* 2004) make them easy to detect. The five others represent clear-sky observations over ocean, dark vegetation, bright vegetation (i.e. sparse vegetation, where the bright underlying soil is visible), dark desert, and bright desert scenes (see Loeb *et al.* 2003). For these six scene types, figure 2(*a*) shows typical simulated average top-of-atmosphere spectral response curves. The clear-sky measurements are obtained by a cloud screening on the original images, following Ipe *et al.* (2003). 219 clear-sky sites, shown in figure 1(*b*), are defined based on their temporal stability (see Decoster *et al.* 2013), and are grouped to create the five clear-sky time series.

The Meteosat level 1.5 images used here are converted from digital counts to radiances using the fixed calibration and offset coefficients at launch,[1] and are rescaled to 5 km resolution by averaging them out spatially. To compare the Meteosat-7 and -8 observations, two corrections are needed. Since the two instruments have different spectral response curves, the first correction consists of converting the original filtered radiances into unfiltered broadband radiances which are independent of the instrument's spectral response curve. This conversion is performed using theoretical regressions obtained from the radiative transfer model libRadtran (Mayer and

Downloaded by [Koninklijk Meteorlogical Institute van] at 02:29 09 October 2013

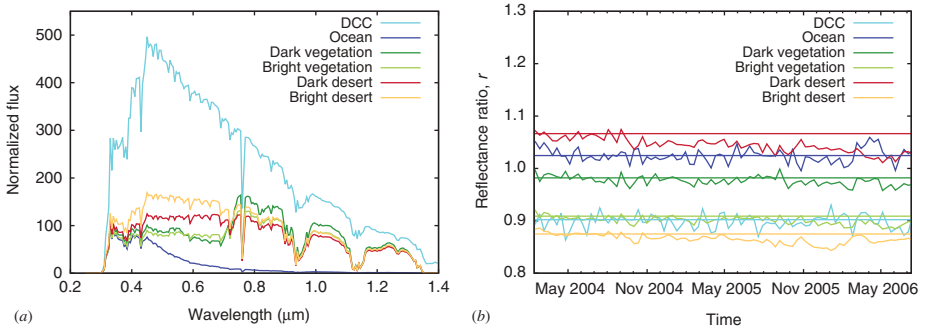

Figure 2. (*a*) Simulated average top-of-atmosphere spectral response curves of the six different scene types used. (*b*) The Meteosat-8 time series expressed in reflectance ratio (r). The horizontal lines show the level of the intercepts $\tilde{r}$.

Kylling 2005), as explained in Decoster *et al.* (2013). The second correction is done to account for small differences in acquisition time and observation geometry between Meteosat-7 and -8. For this, the unfiltered radiances are converted into reflectances, and finally divided by models of broadband bidirectional reflectances provided by Loeb *et al.* (2003) (see equation (7) in Decoster *et al.* (2013)). The obtained reflectance ratios r depart from 1 as the Loeb *et al.* (2003) models are averages over the global tropical domain and not just the Meteosat field of view.

Figure 2(*b*) shows the six reflectance ratio time series $r(t)$ for Meteosat-8. A limited ageing effect is visible, which is assumed to be linear over the first few years of operation. The ageing is corrected by making a linear fit through the time series and using the six intercept values at the beginning of operation (February 2004) as reference for Meteosat-7. The possibility of spectral ageing effects is taken into account by allowing different slopes for each scene type. The values of the intercepts ($\tilde{r}$) are shown in figure 2(*b*) by the horizontal lines. The standard error $s(\tilde{r})$ on each intercept is calculated following Kutner *et al.* (2005):

$$s(\tilde{r}) = \sqrt{\frac{\sum_{i=1}^{m} (r_i - \tilde{r} - bt_i)^2}{m-2} \left(\frac{1}{m} + \frac{\langle t \rangle^2}{\sum_{i=1}^{m} (t_i - \langle t \rangle)^2} \right)} \tag{2}$$

where b is the slope of the linear fit through the time series, r_i is the reflectance ratio at time t_i, m is the number of data points, and $\langle t \rangle$ is the mean of t_i.

In the same way, the intercepts $\tilde{r}$ of the linear fits through the time series are computed for each time series of Meteosat-7, using the same sites as for Meteosat-8. The relative intercept difference $\Delta\tilde{r}/\tilde{r}$ between Meteosat-7 and Meteosat-8, where the latter is used as the reference, and its standard error are calculated as

$$\frac{\Delta\tilde{r}}{\tilde{r}} \pm s\left(\frac{\Delta\tilde{r}}{\tilde{r}}\right) = \frac{\tilde{r}_7 - \tilde{r}_8}{\tilde{r}_8} \pm \frac{\tilde{r}_7 - \tilde{r}_8}{\tilde{r}_8} \sqrt{\left(\frac{s(\tilde{r}_7)}{\tilde{r}_7}\right)^2 + \left(\frac{s(\tilde{r}_8)}{\tilde{r}_8}\right)^2} \tag{3}$$

Downloaded by [Koninklijk Meteorlogical Institute van] at 02:29 09 October 2013

for each time series, where $\tilde{r}_7$ and $\tilde{r}_8$ are the intercepts for Meteosat-7 and Meteosat-8, and $s(\tilde{r}_7)$ and $s(\tilde{r}_8)$ are their standard errors, calculated using equation (2).

3. Results

3.1 *Relative intercept differences*

In figure 3(*a*), the Meteosat-7 reflectance ratio time series are shown together with the horizontal lines indicating the reference intercept values from Meteosat-8. The six time series have been corrected for ageing using the spectral ageing model from equation (1). The $\Delta\tilde{r}/\tilde{r}$ values are given in the first column of table 1 for all six scene types, together with the mean bias $1/n\sum_{i=1}^{n}\Delta\tilde{r}_i/\tilde{r}_i$, mean absolute bias $1/n\sum_{i=1}^{n}\left|\Delta\tilde{r}_i/\tilde{r}_i\right|$, and root mean square (RMS) of the intercept differences $\sqrt{1/n\sum_{i=1}^{n}\left(\Delta\tilde{r}_i/\tilde{r}_i - \text{mean bias}\right)^2}$, with n the number of time series. To validate the use of the spectral ageing model of Decoster *et al.* (2013), the data are in a second step corrected for ageing using the grey model of Govaerts *et al.* (2004) instead. The results are shown in figure 3(*b*) and in the second column of table 1.

As there is doubt about the different features in the blue part of the pre-launch characterization of the Meteosat-7 spectral response curve, and the curve of Meteosat-8 has a much smoother shape, the Meteosat-7 spectral response curve is now replaced

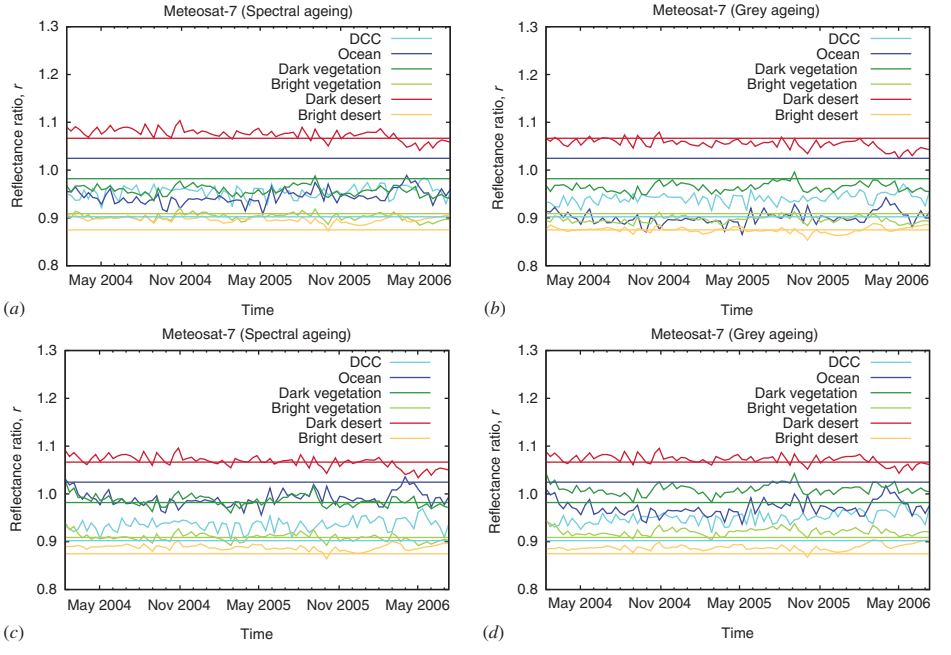

Figure 3. The Meteosat-7 time series expressed in reflectance ratio. The horizontal lines show the value of the intercept of the Meteosat-8 time series, used as reference. (*a*) Meteosat-7 spectral response curve with spectral ageing. (*b*) Meteosat-7 spectral response curve with grey ageing. (*c*) Meteosat-8 spectral response curve with spectral ageing. (*d*) Meteosat-8 spectral response curve with grey ageing.

Downloaded by [Koninklijk Meteorologisch Instituut van] at 02:29 09 October 2013

Table 1. The relative differences between the Meteosat-8 and Meteosat-7 intercepts (columns one through four). Fifth column: relative error contribution to $\Delta\tilde{r}/\tilde{r}$ from the conversion from filtered to unfiltered radiance. Sixth column: relative error contribution from the uncertainty on the Meteosat-8 HRV spectral response curve. Seventh column: total relative error contribution.

	Relative intercept difference $\Delta\tilde{r}/\tilde{r}$ (%)				Relative error contribution (%)		
	Meteosat-7 spectral response		Meteosat-8 spectral response				
	Spectral ageing	Grey ageing	Spectral ageing	Grey ageing	Unfiltering ϵ_u	Meteosat-8 spectral response ϵ_s	Total ϵ
DCC	5.29	3.57	3.14	4.16	0.17	0.35	0.64
Ocean	−8.67	−12.7	−3.69	−5.71	0.87	0.94	1.38
Dark vegetation	−2.09	−2.02	1.01	2.62	0.75	0.45	1.01
Bright vegetation	−0.43	−1.46	0.61	1.24	1.27	0.24	1.38
Dark desert	2.04	−0.15	1.41	1.23	0.74	0.20	0.91
Bright desert	2.80	0.01	1.70	1.11	0.53	0.27	0.78
Mean bias	−0.18	−2.14	0.65	0.73	0.72	0.41	1.02
Mean absolute bias	3.55	3.34	1.88	2.63			
RMS difference	4.46	5.05	2.10	3.09			

by the one of Meteosat-8 to see how this changes the results. As the Meteosat-8 spectral response curve is narrower than the one of Meteosat-7, the calibration coefficient is multiplied by the ratio of the band integrated solar irradiation for both filters (0.85). This means that the ratio is taken of the convolution product of the solar spectrum and the HRV spectral response and of the convolution product of the solar spectrum and the Meteosat-7 visible spectral response. The resulting time series are shown in figures 3(*c*) and 3(*d*), where the Meteosat-7 data has been corrected for ageing using the spectral ageing and the grey ageing models, respectively. The intercept differences are given in the third and fourth column of table 1.

3.2 *Error calculation*

The four major sources contributing to the error on $\Delta\tilde{r}/\tilde{r}$ are: (i) an uncertainty ϵ_u introduced by the conversion from filtered radiances into unfiltered radiances, (ii) the standard error on the intercept values, ϵ_r, (iii) the uncertainty on the Meteosat-8 HRV spectral response curve, ϵ_s, and finally, (iv) the error ϵ_a due to the ageing model on Meteosat-7.

First of all, the relative error ϵ_u, introduced by the conversion from filtered to unfiltered radiances, is calculated. Although the conversion itself introduces errors of about 3–4%, these errors are highly correlated and only about 0.7% of standard error remains in the difference in reflectance ratio $\Delta\tilde{r}/\tilde{r}$. The exact values are given in the fifth column of table 1 for each of the different scene types. Next, the standard errors on the intercepts are computed using equation (2), and converted into the relative standard error ϵ_r on the intercept difference in equation (3). The error is small, with a maximum value over all the scene types of 0.04%. It is this value that is taken into the error budget. An extra error ϵ_s is introduced by the Meteosat-8 HRV spectral response characterization. Using the uncertainty on the HRV response curve provided by Govaerts

Downloaded by [Koninklijk Meteorlogical Institute van] at 02:29 09 October 2013

Table 2. Relative differences between the Meteosat-8 and Meteosat-7 intercepts for IGBP surface classification.

	Relative intercept difference $\Delta\tilde{r}/\tilde{r}$ (%)			
	Meteosat-7 spectral response		Meteosat-8 spectral response	
	Spectral ageing	Grey ageing	Spectral ageing	Grey ageing
DCC	5.29	3.57	3.14	4.16
Ocean	−8.67	−12.7	−3.69	−5.71
Evergreen broadleaf forest	−1.03	−0.83	1.95	3.67
Closed shrublands	−1.89	−3.16	0.37	0.80
Open shrublands	1.00	−0.84	1.05	1.14
Woody savannas	−1.29	−1.58	1.22	2.51
Savannas	−0.34	−1.24	0.93	1.69
Grasslands	0.76	−0.86	0.83	1.06
Croplands	0.83	−0.45	1.43	1.88
Cropland/natural vegetation mosaic	−0.51	−1.18	1.07	2.04
Barren or sparsely vegetated	2.51	−0.04	1.44	1.04
Mean bias	−0.30	−1.76	0.89	1.30
Mean absolute bias	2.19	2.41	1.56	2.34
RMS difference	3.27	3.79	1.60	2.45

et al. (2001), the effect on $\Delta\tilde{r}/\tilde{r}$ is about 0.4%. The ϵ_s values are given in the sixth column in table 1. Finally, in Decoster *et al.* (2013), the residual drift of the Meteosat-7 time series after ageing correction is evaluated as better than 0.075% year^{-1} and so the maximum error ϵ_a due to the ageing model is less than 0.5% after 6 years.

The four error sources are combined using the root square $\left(\epsilon = \sqrt{\epsilon_u^2 + \epsilon_r^2 + \epsilon_s^2 + \epsilon_a^2}\right)$, and are shown in column seven of table 1. The combined error, approximately 1%, represents the total error on the methodology used in this letter. This error magnitude must be taken into account when discussing the results in the next section.

3.3 *Sensitivity to scene type definition*

As an additional verification, the target location is changed and new time series have been constructed for nine land surface types from the International Geosphere/Biosphere Programme (IGBP) (Eidenshink and Faundeen, 1994, Loveland and Belward 1997). The results are provided in table 2. Note that the cloud and clear ocean time series make use of the same sites as before.

4. Discussion

From the first column of table 1, it can be seen that, using the spectral ageing model, the discrepancies between Meteosat-7 and -8 lie between 5.3% (for DCC) and −8.7% (for clear ocean). For land surface, the difference in reflectance ratio remains lower than 3%. While the mean bias is almost equal to zero, the mean absolute bias is equal to 3.5% and the RMS is equal to 4.5%. As this RMS is significantly higher than the 1%

Downloaded by [Koninklijk Meteorlogical Institute van] at 02:29 09 October 2013

error budget, the observed difference between the Meteosat-7 and -8 time series must be attributed to the pre-launch Meteosat-7 spectral response characterization $\phi(\lambda, 0)$.

Comparing the bias and RMS values from the first and second columns shows that the use of the spectral ageing model leads to a better agreement between Meteosat-7 and Meteosat-8. The higher values using the grey ageing model are explained both by the fact that a linear decrease in signal is assumed in the grey model instead of an exponential one, and by the non-correction of the spectral component of the ageing in the grey model.

Whichever ageing model is used, however, the ocean and the cloud signal are clearly lower and higher, respectively, than the corresponding Meteosat-8 values. This could be an indication of an overestimation of the instrument sensitivity in the shortest wavelengths (explaining the negative ocean difference) and an underestimation in the middle of the visible band (explaining the positive cloud difference). As the Meteosat-7 spectral response curve has only been characterized in the 0.5–0.9 μm interval (Govaerts *et al.* 2004), and the rest has been extrapolated, it is not surprising that this extrapolation might not be correct and could be the cause of the strong differences between Meteosat-7 and -8 in the blue part of the spectrum.

Replacing the Meteosat-7 spectral response curve with the one of Meteosat-8 improves the consistency between the two instruments, as can be seen from column three and four of table 1. For the spectral ageing model, the replacement decreases the RMS from 4.5% to 2.1%. A similar improvement is observed for the mean absolute bias. Over the six scene types, the discrepancy between Meteosat-7 and 8 is now in the range of +3.1% to −3.7%. Using the grey ageing model, replacing the Meteosat-7 spectral response curve with the Meteosat-8 curve leads to the same improvement, though slightly less than using the spectral ageing model. Interestingly, it can be seen from figure 1(*a*) that the pre-launch spectral response curve of the Meteosat-7 visible channel presents a higher sensitivity in the blue (around 0.4 μm) and a lower sensitivity in the centre of the channel (0.6 − 0.8 μm) when compared to the curve of the Meteosat-8 HRV channel, which confirms the idea of a possible overestimation of the pre-launch Meteosat-7 response curve at the shortest wavelengths and an underestimation in the middle of the curve.

Table 2 provides evidence that the same conclusions can be drawn when using the IGBP target classification.

5. Conclusion

A method to compare the observations of the Meteosat-7 visible and Meteosat-8 HRV channels has been presented. It involves radiance unfiltering, conversion into reflectance, and normalization with modelled reflectances. Although the overall agreement is good, differences are observed when looking at individual scene types. Using the official EUMETSAT spectral response curve of Meteosat-7 and the grey ageing model, the RMS is 5.2% between the two satellites. Using the spectral ageing model of Decoster *et al.* (2013), the RMS drops to 4.5%. Given that the comparison methodology uncertainty is 1%, this indicates that there is a problem with the pre-launch characterization of the Meteosat-7 spectral response curve. Better agreements are obtained when replacing the Meteosat-7 spectral response curve by the one of Meteosat-8. In this case, the RMS is reduced to 2.1% when using the spectral ageing model.

Downloaded by [Koninklijk Meteorlogical Institute van] at 02:29 09 October 2013

For now, it is suggested to do this replacement for a better interpretation of the Meteosat-7 data record and to improve the consistency with Meteosat-8, when creating climate data records. There is, however, room for improvement. The Scanning Imaging Absorption Spectrometer for Atmospheric Chartography (Sciamachy) could be used as a reference source to correct the Meteosat-7 pre-launch spectral response curve. This way, it should be possible to check if the error in the pre-launch spectral response curve of Meteosat-7 only results from the extrapolation or if there is also a problem in the characterized 0.5–0.9 μm region. It might also be necessary to apply a similar correction to Meteosat-5 and -6 as their current visible characterization relies on the Meteosat-7 spectral response as suggested by Govaerts (1999), though it remains to be confirmed with dedicated sensitivity analyses.

Acknowledgements

The authors would like to thank EUMETSAT for providing help with the research. This work was supported by the Climate Monitoring Satellite Application Facility (CM-SAF) of EUMETSAT.

Note

1. For Meteosat-7 the calibration and offset coefficients are provided by EUMETSAT on their website, for Meteosat-8 they are found in the header of the images.

References

Ba, M.B. and Nicholson, S.E., 1998, Analysis of convective activity and its relationship to the rainfall over the Rift Valley lakes of East Africa during 1983–90 using the Meteosat infrared channel. *Journal of Applied Meteorology*, **37**, pp. 1250–1264.

Decoster, I., Clerbaux, N., Baudrez, E., Dewitte, S., Ipe, A., Nevens, S., Blazquez, A.V. and Cornelis, J., 2013, Modeling the aging effects of Meteosat-7 visible band. *Journal of Atmospheric and Oceanic Technology*, **30**, pp. 496–509.

Desbois, M., Kayiranga, T., Gnamien, B., Guessous, S. and Picon, L., 1988, Characterization of some elements of the Sahelian climate and their interannual variations for July 1983, 1984 and 1985 from the analysis of METEOSAT ISCCP data. *Journal of Climate*, **1**, pp. 867–904.

Doelling, D.R., Nguyen, L. and Minnis, P., 2004, On the use of deep convective clouds to calibrate AVHRR data. In *Proceedings of SPIE*, 5542, 13–17 September 2004, Maspalomas (Gran Canaria: SPIE Press).

Dürr, B., Zelenka, A., Müller, R. and Philipona, R., 2010, Verification of CM-SAF and MeteoSwiss satellite based retrievals of surface shortwave irradiance over the Alpine region. *International Journal of Remote Sensing*, **31**, pp. 4179–4198.

Duvel, J.F. and Kandel, R.S., 1985, Regional-scale diurnal variations of outgoing infrared radiation observed by METEOSAT. *Journal of climate and applied meteorology*, **24**, pp. 335–349.

Eidenshink, J.C. and Faundeen, J.L., 1994, The 1 km AVHRR global land data set: first stages in implementation. *International Journal of Remote Sensing*, **15**, pp. 3443–3462.

Govaerts, Y.M., 1999, Correction of the Meteosat-5 and-6 radiometer solar channel spectral response with the Meteosat-7 sensor spectral characteristics. *International Journal of Remote Sensing*, **20**, pp. 3677–3682.

Govaerts, Y.M., Arriaga, A. and Schmetz, J., 2001, Operational vicarious calibration of the MSG/SEVIRI solar channels. *Advances in Space Research*, **28**, pp. 21–30.

Downloaded by [Koninklijk Meteorlogical Institute van] at 02:29 09 October 2013

GOVAERTS, Y.M. and CLERICI, M., 2003, Evaluation of radiative transfer simulation accuracy over bright desert calibration sites. *Advances in Space Research*, **32**, pp. 2201–2210.

GOVAERTS, Y.M., CLERICI, M. and CLERBAUX, N., 2004, Operational calibration of the meteosat radiometer VIS band. *IEEE Transactions on Geoscience and Remote Sensing*, **42**, pp. 1900–1914.

GOVAERTS, Y.M. and LATTANZIO, A., 2008, Estimation of surface albedo increase during the eighties Sahel drought from Meteosat observations. *Global and Planetary Change*, **64**, pp. 139–145.

IPE, A., CLERBAUX, N., BERTRAND, C., DEWITTE, S. and GONZALEZ, L., 2003, Pixel-scale composite top-of-the-atmosphere clear-sky reflectances for Meteosat-7 visible data. *Journal of Geophysical Research*, **108**, p. 4612.

KUTNER, M.H., NACHTSHEIM, C.J., NETER, J. and LI, W., 2005, *Applied Linear Statistical Models*, 5th ed., Einstein's Legacy (New York: McGraw-Hill).

LOEB, N.G., MANALO-SMITH, N., KATO, S., MILLER, W.F., GUPTA, S.K., MINNIS, P. and WIELIKI, B.A., 2003, Angular distribution models for top-of-atmosphere radiative flux estimation from the clouds and the earth's radiant energy system instrument on the tropical rainfall measuring satellite. Part I: methodology. *Journal of Applied Mateorology*, **42**, pp. 240–265.

LOVELAND, T.R. and BELWARD, A.S., 1997, The IGBP-DIS global 1 km land cover data set, DISCover: first results. *International Journal of Remote Sensing*, **18**, pp. 3289–3295.

MAYER, B. and KYLLING, A., 2005, Technical note: The libRadtran software package for radiative transfer calculations – description and examples of use. *Atmospheric Chemistry and Physics Discussion*, **5**, pp. 1319–1381.

MÜLLER, R.W., MATSOUKAS, C., GRATZKI, A., BEHR, H.D. and HOLLMANN, R., 2006, The CM-SAF operational scheme for the satellite based retrieval of solar surface irradianceA LUT based eigenvector hybrid approach. *Remote Sensing of Environment*, **113**, pp. 1012–1024.

POSSELT, R., MÜLLER, R.W., STÖCKLI, R. and TRENTMANN, J., 2012, Remote sensing of solar surface radiation for climate monitoring – the CM-SAF retrieval in international comparison. *Remote Sensing of Environment*, **118**, pp. 186–198.

ROEBELING, R.A., FEIJT, A.J. and STAMMES, P., 2006, Cloud property retrievals for climate monitoring: implications of differences between Spinning Enhanced Visible and Infrared Imager (SEVIRI) on METEOSAT-8 and Advanced Very High Resolution Radiometer (AVHRR) on NOAA-17. *Journal of Geophysical Research:*, **111** , D20210. doi:10.1029/2005JD006990

SCHMETZ, J., PILI, P., TJEMKES, S., JUST, D., KERKMANN, J., ROTA, S., and RATIER, A., 2002, An introduction to Meteosat second generation (MSG). *Bulletin of the American Meteorological Society*, **83**, pp. 977–992.

SCHULZ, J., ALBERT, P., BEHR, H.-D., CAPRION, D., DENEKE, H., DEWITTE, S., DÜRR, B., FUCHS, P., GRATZKI, A., HECHLER, P., HOLLMANN, R., JOHNSTON, S., KARLSSON, K.-G., MANNINEN, T., MÜLLER, R., REUTER, M., RIIHELÄ, A., ROEBELING, R., SELBACH, N., TETZLAFF, A., THOMAS, W., WERSCHECK, M., WOLTERS, E., and ZELENKA, A 2009, Operational climate monitoring from space: the EUMETSAT satellite application facility on climate monitoring (CM-SAF). *Atmospheric Chemistry and Physics*, **9**, pp. 1687–1709.

VERMOTE, E. and KAUFMAN, Y.J., 1995, Absolute calibration of AVHRR visible and near-infrared channels using ocean and cloud views. *International Journal of Remote Sensing*, **16**, pp. 2317–2340.

Downloaded by [Koninklijk Meteorlogical Institute van] at 02:29 09 October 2013